Electronic Supplementary Material (ESI) for Green Chemistry.
This journal is © The Royal Society of Chemistry 2020

Supplementary Information

for

Practical and inexpensive acid-activated montmorillonite catalysts for energy-efficient CO_2 capture

Umair H. Bhatti[1, 2], Wajahat W. Kazmi[1, 2], Hafiz A. Muhammad[1, 2], Gwan Hong Min[1, 2], Sung Chan Nam[1, 2*], Il Hyun Baek[1, 2*]

[1]Korea Institute of Energy Research, 217 Gajeong-ro Yuseong-gu, Daejeon, 34129, South Korea

[2]University of Science and Technology, 217 Gajeong-ro Yuseong-gu, Daejeon, 34113, South Korea

*Corresponding author email:

Sung Chan Nam: scnam@kier.re.kr

Il Hyun Baek: ihbaek@kier.re.kr

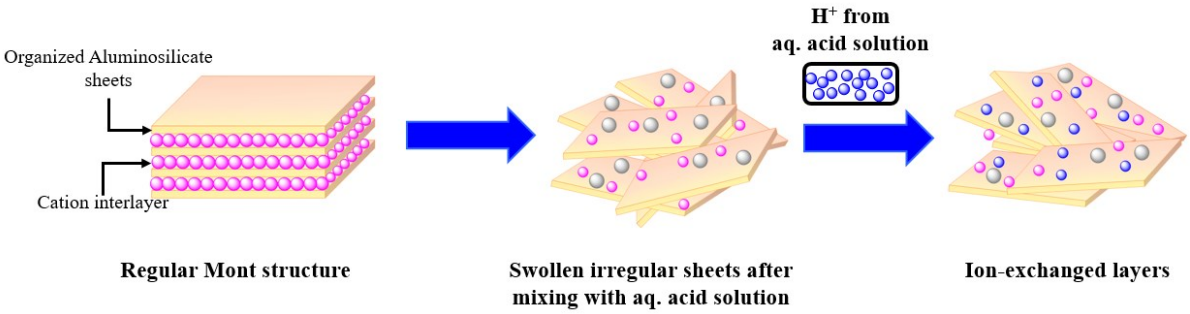

Figure S1. Schematic diagram of the Mont structure and ion exchange process during acid activation

Experimental section:

Montmorillonite (1302-78-9), monoethanolamine (>99%), HCl (37%), HNO_3 (70%), and H_3PO_4 (85%) were purchased from Sigma-Aldrich. CO_2 and N_2 gases (purity of 99.999%) were purchased from Korea Nano Gas Co. Ltd.

Physical characterization

The X-ray diffraction (XRD) patterns were recorded using a Rigaku D/max 2200PC diffractometer equipped with a Cu sealed tube (λ=1.54178 Å) at a scan rate of 0.5^o min^{-1} in the range from 5 to 80^o.

The Brunauer−Emmett−Teller (BET) surface area and porosity of catalysts were determined using the nitrogen adsorption method at −200 °C with a constant volume adsorption apparatus (Micromeritics, ASAP-2420).

The surface density and strength of the acid sites were measure by a temperature-programmed desorption of ammonia apparatus (Micromeritics, Autochem II). Around 0.1 g of the sample was pretreated at 200 ^oC for 2 h in a flow of Helium to clean the surface. The samples were then cooled down to room temperature, and ammonia was introduced into the reactor at 100 ^oC for 1 h.

For Py-FTIR spectroscopy, self-supporting wafers (11 tons cm^{-2}, 30 mg, and 1 cm^2) were pretreated at 300 °C for 2 h under vacuum (10^{-3} mbar) in a stainless steel IR cell. The, hot pyridine vapors at 100 °C were introduced into the IR cell for 2 h until the pressure inside the IR cell reached 5 bar. Then, the IR cell was connected to an infrared spectroscope, and the IR spectra of the materials were recorded in the range of wavenumber 600−4000 cm^{-1} with 8 cm^{-1} optical resolution and co-addition of 32 scans. The quantitative values of Brønsted and Lewis acid sites were calculated using Equation 1 and 2.

$$C(B\ sites) = \frac{1.88IA(B)R^2}{W} \quad (1)$$

$$C(L\ sites) = \frac{1.42IA(L)R^2}{W} \quad (2)$$

where C is the concentration of acid sites (mmol g^{-1} catalyst), IA (B, L) are the integrated absorbance of B or L band (cm^{-1}), R is the radius of catalyst disk (cm), and W = weight of disk (mg).

The surface morphology of the parent and acid-activated Mont catalysts was observed with a scanning electron microscope (SEM; S-4800, Hitachi).

Experimental procedure:

A 250 mL glass reactor was connected to an oil circulator to heat the amine solution. A K-type thermocouple was inserted into the reactor to record the temperature of amine solution. A glass condenser was mounted on the reactor to condense and reflux water and amine vapors. A magnetic stirrer was used at 300 rpm to stir the solution throughout the regeneration experiments. The MEA solution regeneration was studied by heating 100 g of CO_2-rich MEA solution from room temperature to ~86 ^oC. The temperature was then kept constant at 86 ^oC until the released CO_2 was < 0.1%. In the catalytic experiment, 5 wt.% of each catalyst was added to 100 g MEA solution at room temperature. The released CO_2 gas went through a check valve where it was mixed with N_2 carrier gas (50 mL/min) prior its quantitative analysis in a gas chromatograph. The quantity of the desorbed CO_2 was calculated by integrating the CO_2 desorption profiles. The heat duty of solvent regeneration was recorded using a power meter (Wattman HPM-100A) which was connected with the heating oil circulator.

The heat duty (KJ/mol CO_2) of MEA solvent regeneration was calculated using Equation 3. The heat duty was determined by dividing the power consumption by the total quantity of CO_2 released during the regeneration experiments.

$$HD = \frac{Heat\ input\ (KJ)}{Quantity\ of\ desorbed\ CO_2\ (mol)} \quad (3)$$

For better comparison of the catalytic and non-catalytic systems, the use of relative heat duty was adopted, as previously suggested by Liang et al.[1] The relative heat duty of solvent regeneration was defined as shown in Equation 4.

$$RHD = \frac{HD_{cat}}{HD_{baseline}} * 100 \quad (4)$$

where RHD is the relative heat duty (%), and $HD_{baseline}$ and HD_{cat} are the heat duties for the non-catalytic and catalytic MEA solutions respectively.

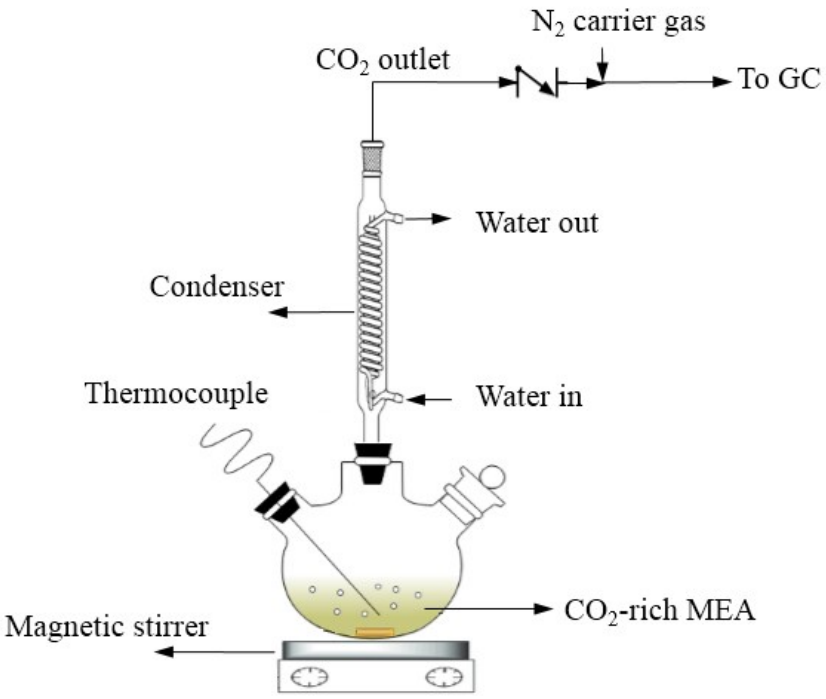

Figure S2. Schematic diagram of the experimental apparatus used to perform solvent regeneration

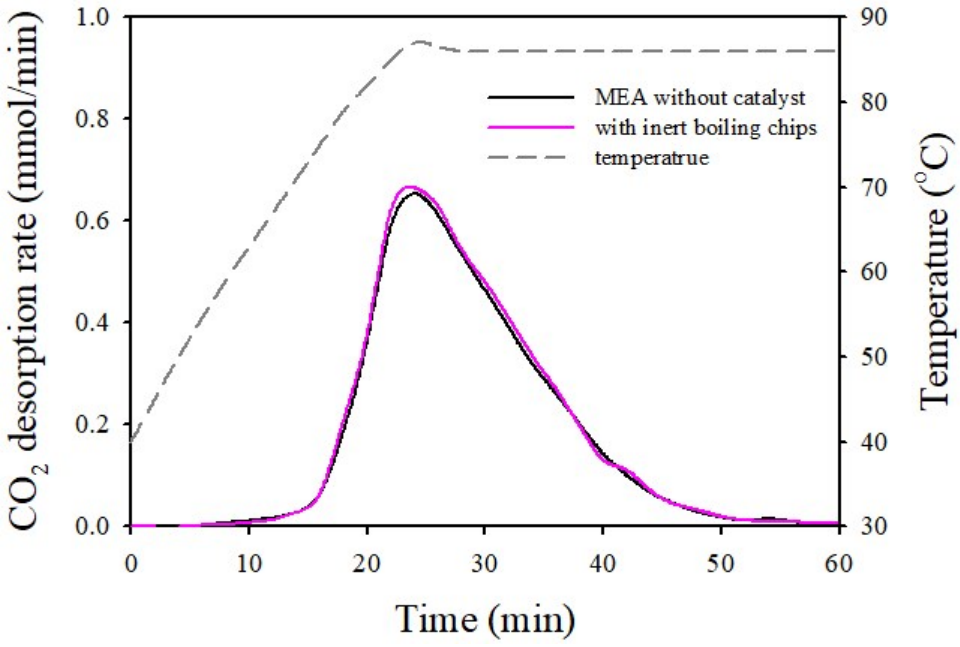

Figure S3. CO_2 desorption rate curves for MEA solution regeneration without and with 5 wt.% inert microporous chips

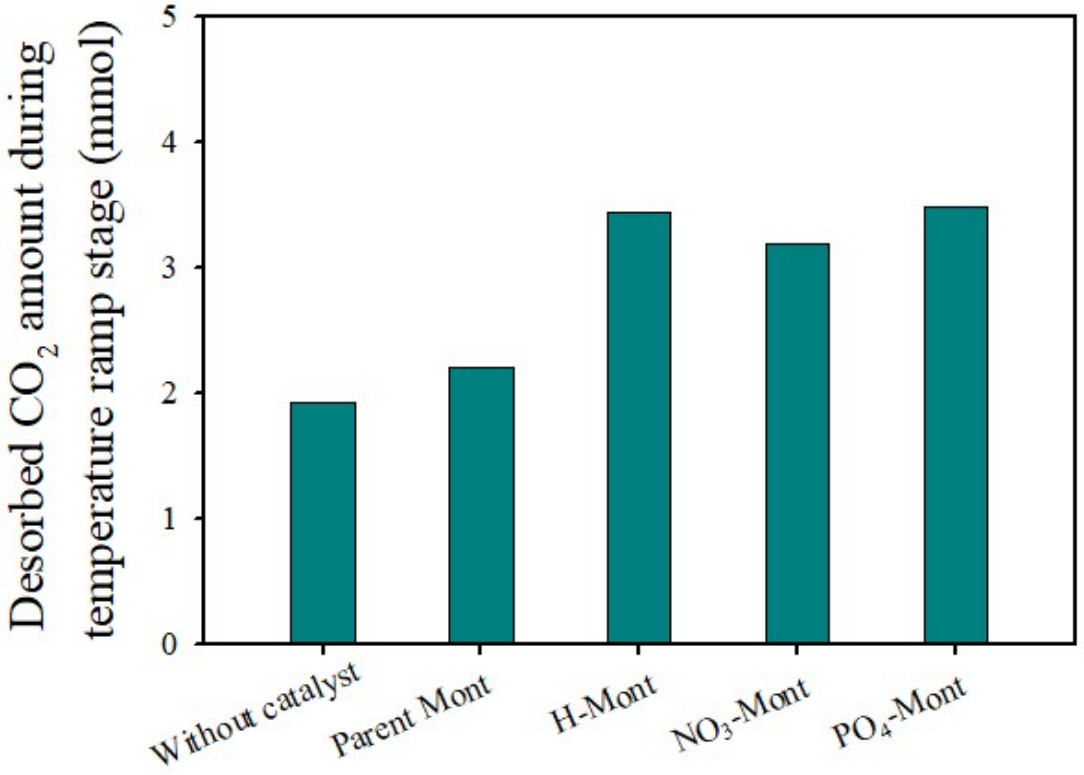

Figure S4. Total amount of CO_2 desorbed from MEA solutions without and with catalysts during temperature ramp stage

Effect of various physicochemical properties on MEA regeneration performance:

The impact of physicochemical properties of the catalysts on the CO_2 desorption performance was evaluated by considering multiple single properties (such as BET surface area, mesoporosity, Total acidity, and total acid sites) and combination of various properties (such as MSA × total acidity and MSA × (LAS+BAS)). The obtained results are presented in Figure S5. It can be seen the BET surface area and the mesoporous surface area have identical patterns, and they completely fit the CO_2 desorption performance of the prepared catalysts. In addition, the combination of MSA with total acidity (calculated from NH_3-TPD) and with total acid sites (LAS+BAS) also proved to completely match the CO_2 desorption performance. This shows that the catalytic performance of the acid-activated Mont catalysts was mainly dependent on the surface area, mesoporosity, and concentration of acid sites. Regarding the effect of total

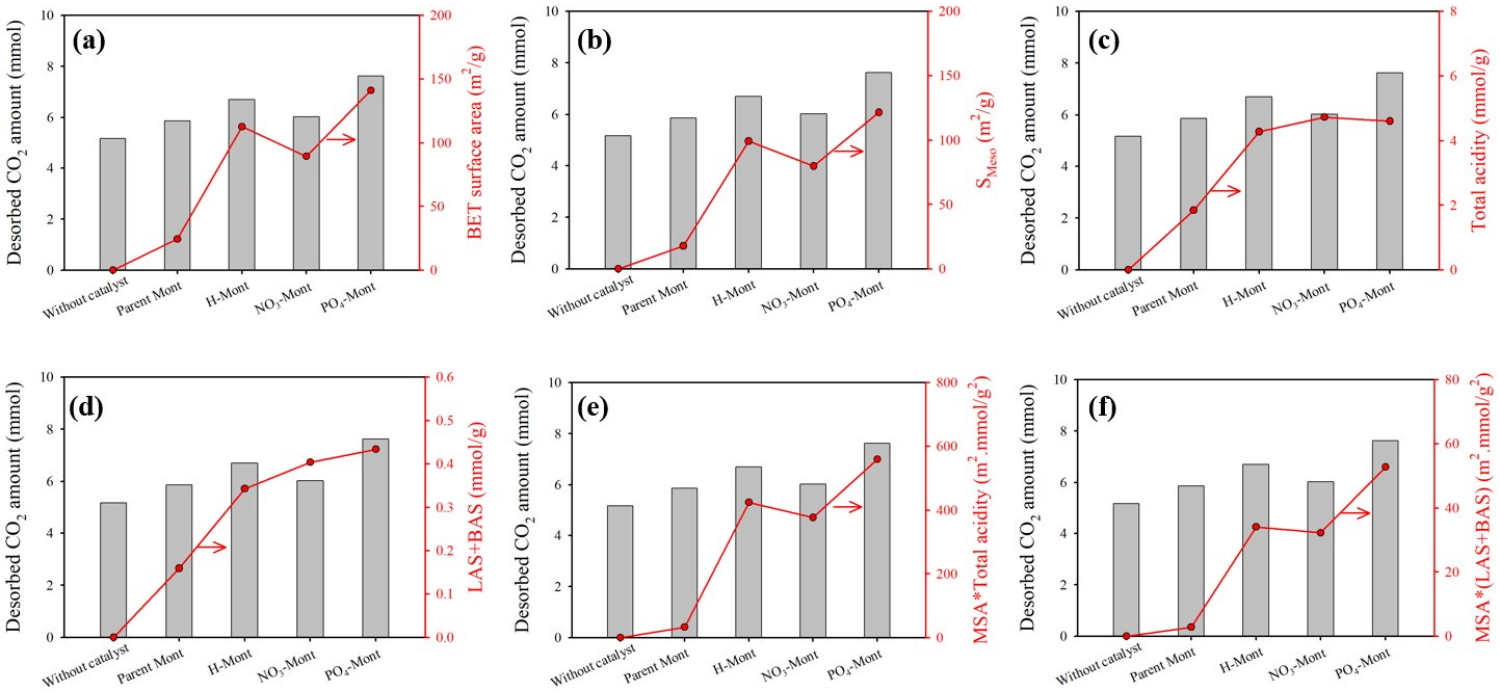

Figure S5. Influence of single and combined catalyst properties on the CO_2 desorption performance (a) influence of BET surface area (b) influence mesoporous area (c) influence of total acidity determined by NH3-TPD (d) influence of total acid sites (LAS and BAS) determined by Py-IR (e) influence of MSA × total acidity and (f) influence of MSA × total acid sites(LAS and BAS)

acidity and total acid sites on the CO_2 desorption performance, an increase in acidity favors the CO_2 desorption; however, this trend is not linear. In fact, NO_3-Mont catalyst had a higher surface acidity than the PO_4-Mont catalyst, but it released a lower quantity of CO_2 than that from PO_4-Mont.

Scanning Electron Microscopy analysis:

The topographical features of the parent and acid-activated Mont catalysts were studied by Scanning Electron Microscopy (SEM) analysis. The parent Mont had a flake-like layered structure. After activation with HCl, HNO_3, and H_3PO_4 acid solutions, almost similar flake-like morphologies were observed, which indicated that treatment with acid solutions had a limited effect on Mont morphology.

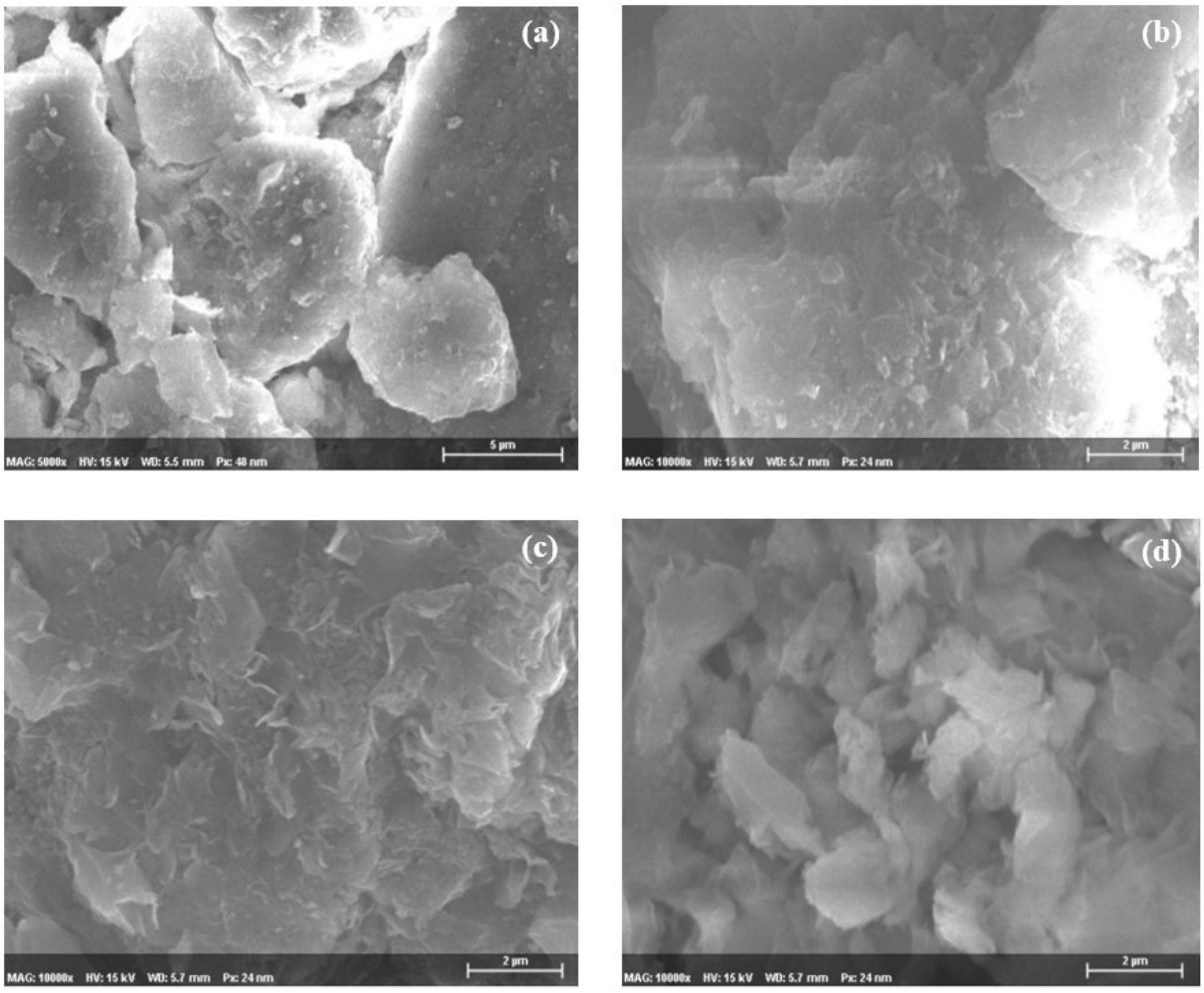

Figure S6. SEM images of the parent and acid-activated Mont catalyst **(a)** parent Mont **(b)** H-Mont **(c)** NO_3-Mont and **(d)** PO_4-Mont

FTIR analysis:

The FTIR spectra for the parent and acid-activated Mont catalysts are shown in Figure S7. The FTIR bands at 457, 516, 621, and 840 cm^{-1} were attributed to Si−O−Si, Al−O−Si, Al−O, and Al−OH−Mg vibrations, respectively[2,3]. The most prominent difference in the acid-activated Mont catalysts was the complete disappearance of Al−OH−Mg at 840 cm^{-1}. Another noticeable difference is the slight reduction in the intensity of the Si−O band at 996 cm^{-1} for the acid-activated catalyst. Moreover, this peak at 996 cm^{-1} also slightly shifted to around 1020 cm^{-1} for acid-activated catalysts mainly due to the increase in the relative amount of silica in the activated Mont.

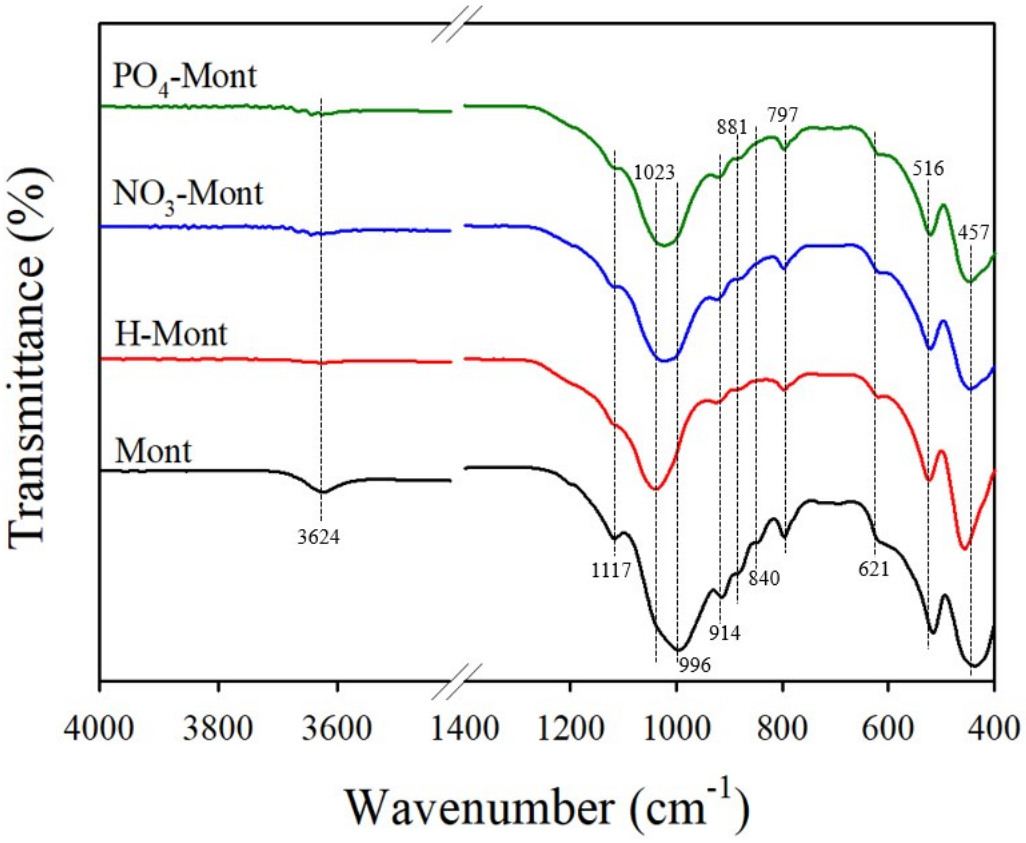

Figure S7. FTIR spectra for the parent and acid-activated Mont catalysts

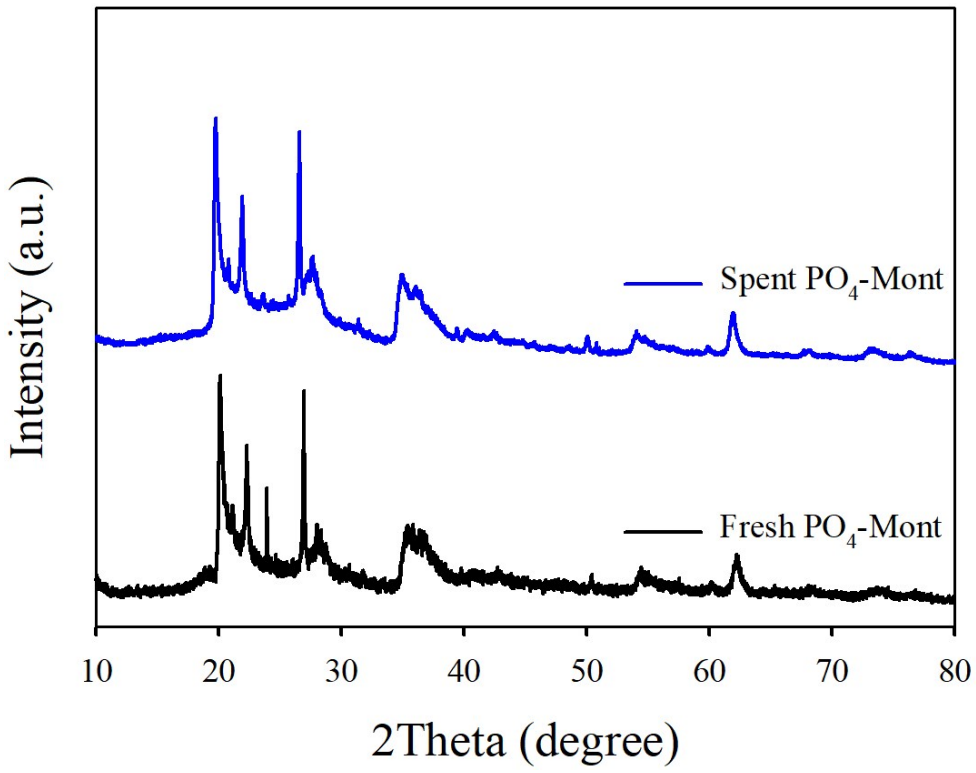

Figure S8. XRD patterns of the fresh and used PO_4-Mont catalyst

Table S1: Comparison with catalytic CO_2 desorption performance of reported catalysts

Catalyst	Solution	Desorption temp. (°C)	Results	References
SO_4^{2-}/TiO_2	MEA	95	CO_2 desorption rate increased by 28.9%	Li et al.[4]
ZrO_2, ZnO	MEA	86	Desorption rate optimized by up to 54%	Bhatti et al.[5]
SAPO-34, SO_4^{2-}/TiO_2	MEA	96	Heat duty reduced by up to 24.3%	Zhang et al.[6]
Cu metal ions	MEA	80	Heat duty reduced by 13.2-24%	Cheng et al.[7]
Fe Promoted SO_4^{2-}/ZrO_2/MCM-41	MEA	98	Desorption factor increased by 260-388%	Zhang et al.[8]
HZSM-5, γ-Al_2O_3	MEA	95	Heat duty reduced by ~30%	Srisang et al.[9]
bifunctional Al_2O_3/HZSM-5	MEA	96	Heat duty reduced by 23-34%	Zhang et al.[10]
Acid-activated Montmorillonite	MEA	86	CO_2 desorption rate improved up to 180%	This work

References:

1 H. Gao, Y. Huang, X. Zhang, Z. A. S. Bairq, Y. Huang, P. Tontiwachwuthikul and Z. Liang, *Appl. Energy*, 2020, **259**, 114179.

2 L. Zatta, L. P. Ramos and F. Wypych, *J. Oleo Sci.*, 2012, **61**, 497–504.

3 L. Zatta, L. P. Ramos and F. Wypych, *Appl. Clay Sci.*, 2013, **80**–**81**, 236–244.

4 L. Li, Y. Liu, K. Wu, C. Liu, S. Tang, H. Yue, H. Lu and B. Liang, *Greenh. Gases Sci. Technol.*, 2020, **10**, 449–460.

5 U. H. Bhatti, S. Nam, S. Park and I. H. Baek, *ACS Sustain. Chem. Eng.*, 2018, **6**, 12079–12087.

6 X. Zhang, X. Zhang, H. Liu, W. Li, M. Xiao, H. Gao and Z. Liang, *Appl. Energy*, 2017, **202**, 673–684.

7 C. hung Cheng, K. Li, H. Yu, K. Jiang, J. Chen and P. Feron, *Appl. Energy*, 2018, **211**, 1030–1038.

8 X. Zhang, Z. Zhu, X. Sun, J. Yang, H. Gao, Y. Huang, X. Luo, Z. Liang and P. Tontiwachwuthikul, *Environ. Sci. Technol.*, 2019, **53**, 6094–6102.

9 W. Srisang, F. Pouryousefi, P. A. Osei, B. Decardi-Nelson, A. Akachuku, P. Tontiwachwuthikul and R. Idem, *Chem. Eng. Sci.*, 2017, **170**, 48–57.

10 X. Zhang, H. Liu, Z. Liang, R. Idem, P. Tontiwachwuthikul, M. Jaber Al-Marri and A. Benamor, *Appl. Energy*, 2018, **229**, 562–576.